nature genetics

Reticular dysgenesis (aleukocytosis) is caused by mutations in the gene encoding mitochondrial adenylate kinase 2

Ulrich Pannicke[1,8], Manfred Hönig[1,2,8], Isabell Hess[3], Claudia Friesen[4], Karlheinz Holzmann[5], Eva-Maria Rump[6], Thomas F Barth[7], Markus T Rojewski[1,6], Ansgar Schulz[2], Thomas Boehm[3], Wilhelm Friedrich[2] & Klaus Schwarz[1,6]

Human severe combined immunodeficiencies (SCID) are phenotypically and genotypically heterogeneous diseases[1]. Reticular dysgenesis is the most severe form of inborn SCID. It is characterized by absence of granulocytes and almost complete deficiency of lymphocytes in peripheral blood, hypoplasia of the thymus and secondary lymphoid organs, and lack of innate and adaptive humoral and cellular immune functions, leading to fatal septicemia within days after birth[2–8]. In bone marrow of individuals with reticular dysgenesis, myeloid differentiation is blocked at the promyelocytic stage, whereas erythro- and megakaryocytic maturation is generally normal. These features exclude a defect in hematopoietic stem cells but point to a unique aberration of the myelo-lymphoid lineages. The dramatic clinical course of reticular dysgenesis and its unique hematological phenotype have spurred interest in the unknown genetic basis of this syndrome. Here we show that the gene encoding the mitochondrial energy metabolism enzyme adenylate kinase 2 (AK2) is mutated in individuals with reticular dysgenesis. Knockdown of zebrafish *ak2* also leads to aberrant leukocyte development, stressing the evolutionarily conserved role of AK2. Our results provide *in vivo* evidence for AK2 selectivity in leukocyte differentiation. These observations suggest that reticular dysgenesis is the first example of a human immunodeficiency syndrome that is causally linked to energy metabolism and that can therefore be classified as a mitochondriopathy.

Reticular dysgenesis or aleukocytosis (MIM267500) is the most severe human primary combined immunodeficiency and accounts for less than 2% of SCID. We studied six individuals with reticular dysgenesis from five independent families (**Supplementary Table 1** online). In three of the families there is evidence of consanguinity (**Supplementary Fig. 1** online). Known causes of SCID were excluded by genetic and functional analyses. Assuming a recessive inheritance model, we conducted a screening for homozygous chromosomal regions using genome-wide SNP analysis with DNA obtained from the six individuals. In four families (including those with consanguinous parents), this analysis revealed a common region on chromosome 1p34.3–1p36.11, where none of the markers showed evidence of heterozygosity. This region was flanked by *C1orf135* on the telomeric side of the critical interval and by *CSF3R* on the centromeric side. This region encompassed 185 genes, 80 of which were expected to be expressed in bone marrow according to the UniGene expression database. We examined the expression of these 80 genes in bone marrow mononuclear cells (MNC) derived from the index individual of family 3 (F3P1) by RT-PCR. When we compared the amplification products to those obtained from a healthy subject, we found that the cDNAs encoding adenylate kinase 2 (AK2) revealed smaller products than the expected 815-bp amplimer (primer pair RD60F/RD60R; **Fig. 1**), suggesting this gene as a potential candidate locus. Indeed, when we sequenced the exons and splice junctions of the *AK2* gene from genomic DNA of all affected individuals, we detected one missense mutation, two small and one large deletion and two splice site mutations (**Fig. 1a** and **Table 1**). Subject F1P1 bears a homozygous 5,038-bp deletion encompassing parts of exon 6, all of intron 6 (IVS6) and parts of exon 7 reaching into the 3′ UTR of *AK2* (**Supplementary Fig. 2** online). F2P1 is a compound heterozygote with one mutation that eliminates the ATG initiation codon and a second mutation that is a small deletion in exon 2. F3P1 is homozygous for a splice acceptor mutation in IVS3, F4P1 and F4P2 are homozygous for a small deletion in exon 5, and F5P1 is a homozygote for a splice donor mutation in IVS5 (**Fig. 1a** and **Table 1**). We sequenced DNA from available parents and found them to be heterozygous for the mutations, excluding the occurrence of *de novo*

[1]Institute for Transfusion Medicine, University of Ulm, 89081 Ulm, Germany. [2]University Children's Hospital Ulm, 89075 Ulm, Germany. [3]Max-Planck-Institute of Immunobiology, 79108 Freiburg, Germany. [4]Institute of Legal Medicine, University Hospital, 89075 Ulm, Germany. [5]Chip Facility/ZKF, University Hospital Ulm, 89069 Ulm, Germany. [6]Institute for Clinical Transfusion Medicine and Immunogenetics Ulm, German Red Cross Blood Service Baden-Wuerttemberg-Hessen, 89081 Ulm, Germany. [7]Institute for Pathology, University Hospital Ulm, Ulm 89081, Germany. [8]These authors contributed equally to this work. Correspondence should be addressed to K.S. (klaus.schwarz@uni-ulm.de).

Received 24 July; accepted 26 September; published online 30 November 2008; doi:10.1038/ng.265

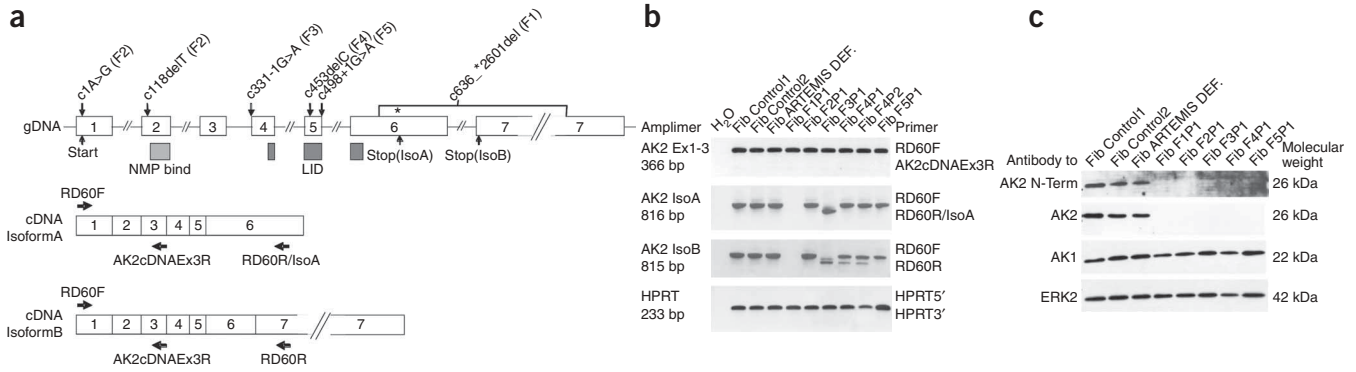

Figure 1 *AK2* mutations and RNA and protein analyses in individuals with reticular dysgenesis. (**a**) *AK2* gene locus, RNA isoforms and mutations in families F1–F5. The AK2 nucleoside monophosphate binding (NMPbind) and LID domain (closes over the ATP substrate) are shown. Splice variants (IsoA and IsoB) of *AK2* and cryptic splice donor site for IsoB in exon 6 (asterisk) are depicted. (**b**) RT-PCR from fibroblasts of control and affected individuals. Primers used and amplimer sizes are indicated. (**c**) Immunoblot of lysates (10 μg) from fibroblasts of affected individuals. Antisera directed against the N-terminal 100 amino acids (AK2 N-Term), or complete AK2 and AK1 were used for detection. ERK2 staining served as loading control. Fibroblasts of two healthy and an ARTEMIS-deficient subject were used for control.

mutations in the affected individuals and supporting an autosomal recessive inheritance model (**Supplementary Fig. 1**). None of these mutations was detected in 112 German (all *AK2* exons) and 50 Turkish (*AK2* exon 5) healthy subjects. One nonconsangineous individual assigned as having reticular dysgenesis did not show any mutations in *AK2* (data not shown).

The mutations did not show any influence on *AK2* steady-state RNA levels, as indicated by RT-PCR with cDNAs generated from primary fibroblast lines of affected individuals (**Fig. 1b**). When we interrogated the expression of the two known full-length AK2 isoforms (isoforms A and B) with two different sets of primers, we did not detect a signal in F1P1 because of the lack of the 3′ primer binding site, whereas subjects F3 to F5 showed varying degrees of aberrant splicing patterns (**Fig. 1b**). The sequences of the RT-PCR products confirmed the mutations and allowed us to characterize the alternative or aberrant splice products of the subjects with splice site mutations (**Supplementary Fig. 3** online). The reason why the IVS3 acceptor splice site mutation of F3P1 and the small deletion in exon 5 in the F4 subjects leads to the identical isoform B splice variant 1 is not yet known.

As assessed by protein blotting with different monoclonal antibodies generated against the AK2 N terminus or the complete AK2 protein, all mutations led to a complete loss of detectable AK2 protein in fibroblasts (**Fig. 1c**), and in MNC of bone marrow (**Fig. 2a**). Thus, we conclude that individuals with reticular dysgenesis bear null mutations in the *AK2* gene.

To independently confirm the function of AK2 in leukocyte development, we examined its role in the zebrafish embryo. As expected for an essential enzyme in energy metabolism, the derived protein sequence of the single *ak2* gene in *Danio rerio* is highly similar to that of human *AK2* and its gene structure is identical (**Supplementary Fig. 4** online). It was possible therefore to mimic one of the mutations in human (F3P1) by designing a splice-site morpholino for the splice acceptor site of intron 3. As expected, this led to aberrant splicing of the zebrafish *ak2* gene predicted to result in the translation of a nonfunctional protein. Interference with ak2 function does not affect the overall development of embryos; likewise, neither immature hematopoietic cells (detected here by expression of scl) nor erythropoiesis, as evidenced by the presence of circulating red blood cells (**Fig. 3** and **Supplementary Fig. 4**), are affected in morphants. By contrast, developing lymphocytes (best revealed by the appearance of T cells in the thymus anlage and detected here by expression of ikaros and rag1) are absent in the *ak2* morphants (**Fig. 3**, **Supplementary Fig. 4** and **Supplementary Table 2** online). This indicates that the phenotype has a high degree of specificity and that ak2 has an evolutionarily conserved function in leukocyte development.

Mitochondrial oxidative phosphorylation (OXPHOS) supplies most of the cellular energy in the form of ATP. The components of the OXPHOS system are encoded by both nuclear and mitochondrial genes. Over 50 mutations in these genes have been linked to rare inborn diseases[9,10], the cardinal clinical features of which are encephalomyopathy and often lactic acidosis. Intracellular energetic balance is facilitated by enzymatic networks comprising adenylate kinases (including AK1 and AK2), creatine kinases (CK), nucleotide diphosphate kinase (NDPK), carbonic anhydrase and glycolytic enzymes, which all support high-energy phosphoryl transfer between ATP-generating and ATP-consuming or sensing sites[11]. AK2 is an ADP-generating enzyme located in the mitochondrial intermembrane space that catalyzes the reversible transfer of a phosphoryl group from ATP to AMP via the reaction ATP-Mg^{2+} + AMP ↔ ADP-Mg^{2+} + ADP[12]. ADP-ATP carriers transport ADP into the mitochondrial matrix and by exchange export ATP synthesized in the OXPHOS reaction out of

Table 1 ***AK2*** **mutations in individuals with reticular dysgenesis**

Subject	Sex	Allele	Mutation	Predicted effect on RNA or protein	Detectable protein
F1P1	Male	M	636_*2601del	Ser213AspfsX21	No
		P	636_*2601del	Ser213AspfsX21	
F2P1	Male	M	118delT	Cys40ValfsX5	No
		P	1A>G	Met1Val	
F3P1	Male	M	331-1G>A	Aberrant splicing	No
		P	331-1G>A	Aberrant splicing	
F4P1	Male	M	453delC	Tyr152ThrfsX12	No
		P	453delC	Tyr152ThrfsX12	
F4P2	Female	M	453delC	Tyr152ThrfsX12	No
		P	453delC	Tyr152ThrfsX12	
F5P1	Female	M[a]	498+1G>A	Aberrant splicing	No
		P[a]	498+1G>A	Aberrant splicing	

Maternal (M) or paternal (P) alleles are indicated. Mutation is denoted as nucleotide sequence in *AK2* cDNA; the adenosine of the initiation codon is nucleotide +1.
[a]In this individual, inheritance was deduced on the basis of consanguinity. The effect of the mutations on RNA or protein is predicted. Protein expression is indicated as assessed by protein blotting of primary fibroblast lysates.

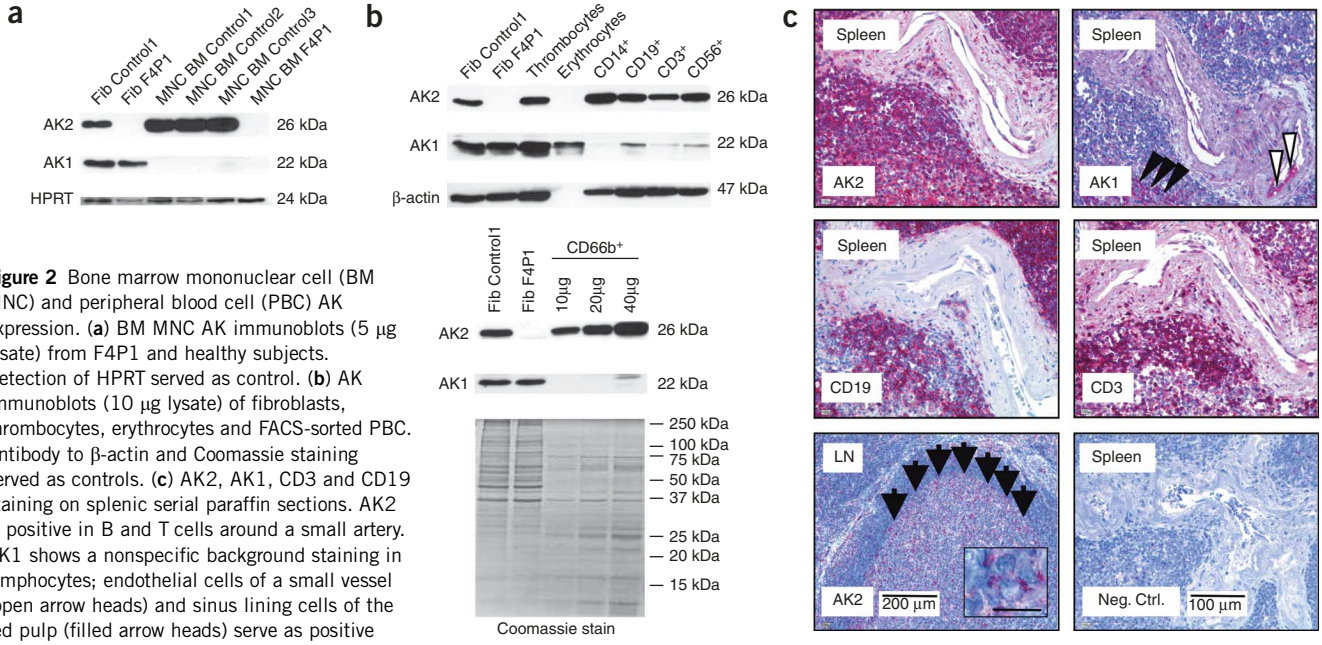

Figure 2 Bone marrow mononuclear cell (BM MNC) and peripheral blood cell (PBC) AK expression. (**a**) BM MNC AK immunoblots (5 µg lysate) from F4P1 and healthy subjects. Detection of HPRT served as control. (**b**) AK immunoblots (10 µg lysate) of fibroblasts, thrombocytes, erythrocytes and FACS-sorted PBC. Antibody to β-actin and Coomassie staining served as controls. (**c**) AK2, AK1, CD3 and CD19 staining on splenic serial paraffin sections. AK2 is positive in B and T cells around a small artery. AK1 shows a nonspecific background staining in lymphocytes; endothelial cells of a small vessel (open arrow heads) and sinus lining cells of the red pulp (filled arrow heads) serve as positive intrinsic controls. A lymph node (LN) germinal center is AK2 positive with weak staining of the mantle (germinal center marked by arrows). Inset, germinal center cell with granular cytoplasmic staining (scale bar, 10 µm). Tumor-free lymphnode biopsies and spleen tissue were obtained from routine diagnostics. The material was anonymized to comply with the German law for correct usage of archival tissue for clinical research.

the matrix into the cytosol. Because ATP synthesis directly depends on the matrix concentration of ADP, the OXPHOS reaction may fail in the absence of adenylate kinases.

Why does loss of function of AK2 lead to such a specific phenotype, considering its central role in energy metabolism? To address this question, we examined the possibility that cytosolic AK1 might compensate, at least partially, for AK2 function. To this end, we analyzed the expression of AK1 and AK2 in different tissues and cell populations of peripheral blood and bone marrow mononuclear cells. Co-expression of AK1 and AK2 was found in all tissues tested (**Supplementary Fig. 5** online). The highest concentrations of AK2 protein were detected in liver and kidney, and the lowest concentrations in brain, skeletal muscle and skin. The various leukocyte-containing tissues expressed comparable amounts of AK2. AK1 expression was strong in skeletal muscle, pancreas and thyroid, whereas the other tissues tested expressed lower but detectable levels of AK1 (**Supplementary Fig. 5**). In peripheral blood erythrocytes and thrombocytes, as well as in nucleated cells sorted by flow cytometry into $CD14^+$, $CD19^+$, $CD3^+$, $CD56^+$ and $CD66b^+$ cells, amounts of AK1 and AK2 varied considerably. Although thrombocytes expressed both AK1 and AK2, erythrocytes, which lack mitochondria, did not show AK2 expression. In contrast, all nucleated cell populations from blood contained readily detectable AK2 protein, but expressed little or no AK1 protein (**Fig. 2b**). This finding was supported by immunohistochemical analyses of spleen and lymph nodes (**Fig. 2c**). Mononuclear cells obtained from bone marrow of healthy donors lacked AK1, whereas AK2 was readily detectable (**Fig. 2a**). These results indicate that leukocytes may be susceptible to defects caused by the lack of AK2, as they do not express AK1 in sufficient amounts to compensate for the AK2 functional deficits.

Judging from the clinical features of individuals with reticular dysgenesis surviving after successful bone marrow transplantation, the only other cell types that are equally susceptible to loss of AK2 function are involved in the organogenesis of the inner ear (**Supplementary Table 1**)[13].

Mitochondria are key regulators of the intrinsic apoptosis pathway, which is initiated through the opening of the mitochondrial permeability transition pore (mtPTP)[10,14,15], a process which can be

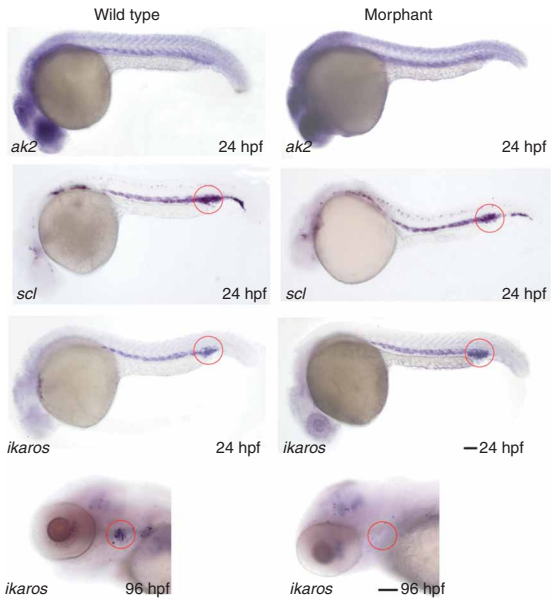

Figure 3 Phenotype of *ak2* zebrafish morphants. In embryos at 24 h postfertilization (hpf), the level of *ak2* mRNA and the expression patterns of *scl* and *ikaros*, which serve as markers for early hematopoiesis, are depicted. The region of the intermediate cell mass is encircled. At 96 hpf, *ikaros* expression in the thymus (red circles) was analyzed. Scale bar, 250 µm in the panels with 24 hpf embryos; 300 µm in the panels with 96 hpf embryos.

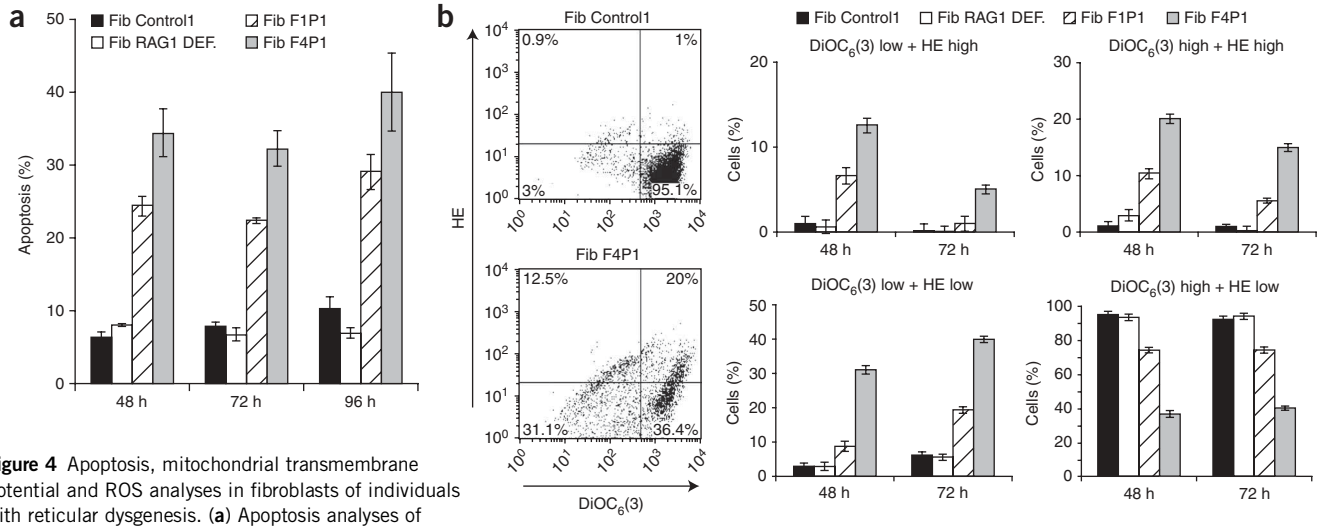

Figure 4 Apoptosis, mitochondrial transmembrane potential and ROS analyses in fibroblasts of individuals with reticular dysgenesis. (**a**) Apoptosis analyses of fibroblasts. The percentage of apoptotic cells was measured by hypodiploid DNA (sub-G1) flow cytometry analysis. Harvest times after plating of viable cells are indicated. Cells of a healthy subject and a RAG1-deficient individual served as controls. Bars represent the means of two triplicate experiments. (**b**) Flow cytometry analyses of fibroblasts after HE (indicates radical oxygen species, ROS) and $DiOC_6(3)$ (a marker for the mitochondrial membrane potential) staining. The dot blots were generated 48 h after plating. Bars, mean of three experiments ± s.d.

stimulated by, for example, decreased mitochondrial ADP. As cells of individuals with reticular dysgenesis lack AK2 function, which contributes about 60% of the ADP flux into the matrix, we assayed cells of individuals with reticular dysgenesis for apoptosis. Spontaneous apoptosis was markedly higher in cultures of fibroblasts from subjects with reticular dysgenesis as compared to controls (25–40% versus 10% or less; **Fig. 4a**). Thus, in fibroblasts AK2 shows an antiapoptotic function. In contrast to controls, no substantial additional increase in apoptosis was seen after etoposide exposition (**Supplementary Fig. 6** online). Furthermore, the number of fibroblasts of individuals with reticular dysgenesis with normal reactive oxygen species production and normal mitochondrial membrane potential was notably lower (**Fig. 4b**).

The propensity for apoptosis may also increase, when the percentage of mutant mtDNA increases, followed by a decline of mitochondrial energetic capacity and higher production of reactive oxygen species[10]. As various primary genetic defects with mtDNA deletions have been described that affect either mitochondrial nucleotide metabolism or mtDNA maintenance[16], we tested fibroblasts of subjects with reticular dysgenesis for quantitative and qualitative mtDNA variations. We did not detect any differences in mtDNA content or integrity as compared to control cells (**Supplementary Fig. 7** online), excluding disturbed mtDNA as a contributor to the reticular dysgenesis phenotype.

We have shown here that mutations in *AK2* are the cause of reticular dysgenesis. Our findings demonstrate that a mitochondriopathy is the cause of a severe immunodeficiency, thus suggesting new avenues, such as gene therapy, for the treatment of this devastating disease.

METHODS

Subjects. The cohort of subjects was recruited at the Children's Hospital Ulm, Germany. The parents of the subjects gave informed consent to the procedures and analyses in accordance to a protocol approved by the local medical review board.

Cell lines. Primary dermal fibroblast cell lines were established from small skin samples explanted during a catheter implantation in all subjects except for F1P4, from whom a bone marrow fibroblast line was cultured. Fibroblasts were grown in DMEM supplemented with 10% FCS.

Genomic DNA preparation. We prepared genomic DNA using either the QIAamp DNA Blood Kit (Qiagen) or the Wizard Genomic DNA Purification Kit (Promega).

SNP analysis and homozygosity determination. Genotyping was done on the Affymetrix GeneChip platform using the 250K *Sty*I array of the Affymetrix 500K system, which consists of 238,000 SNPs (Affymetrix). We subject 250 ng of DNA to restriction endonuclease digestion by *Sty*I and processed the products according to the manufacturer's instructions. A complete protocol (low-throughput method) is available at the Affymetrix website. Arrays were hybridized, stained, washed and scanned using a Hybridization Oven 640, Fluidics station FS450 and a GeneChip Scanner 3000 7G according to the instructions of the manufacturer. Genotying was done on the GTYPE Software 4.0 using the RLMM genotype calling algorithm. We detected homozygous regions using CNAT4.1 (Affymetrix) and visualized them with the IdeogramBrowser[17].

RNA isolation and RT-PCR. RNA was isolated with the RNeasy Mini Kit (Qiagen) followed by DNAse digestion. We reverse-transcribed 200 ng (bone marrow) or 1,000 ng (fibroblasts) total RNA with the SuperScript II Reverse Transcriptase Kit (Invitrogen) with random hexamer priming. For the bone marrow expression screen, bone marrow cDNA of subject F3P1 and a healthy subject was amplified with 80 oligonucleotide pairs of the candidate genes in the homozygous overlap region. Primers and conditions are available on request. For RT-PCR analyses of fibroblasts from affected individuals, the primers used are summarized in **Supplementary Table 3** online.

Genomic sequencing. For *AK2* exon sequencing 100 ng genomic DNA was amplified and sequenced (see **Supplementary Table 3** for primers) with a Big Dye Terminator v1.1 Cycle Sequencing Kit (Applied Biosystems). We separated sequence products on an Applied Biosystems Prism 3100C Genetic Analyzer.

Deletion analysis in family F1. To identify the breakpoint of the deletion in F1, we used PCR and primer walking. The breakpoint was confirmed by a deletion-specific PCR and sequencing (primers listed in **Supplementary Fig. 2** and **Supplementary Table 3**).

Cloning of cDNA products. cDNA products were purified with QIAquick PCR Purification Kit (Qiagen) and cloned into pCR2.1-TOPO-Vector using the

TOPO TA Cloning Kit (Invitrogen). Plasmids were purified with R.E.A.L. Prep96 Plasmid Kit (Qiagen) and sequenced with the primers used for generating the PCR products.

Immunohistochemistry. We used serial paraffin sections of spleen and lymph nodes obtained from routine diagnostic specimens for immunohistochemistry. Polyclonal antibodies to AK1 (1:80, Santa Cruz Biotechnology) and AK2 (1:80, ProteinTech Group) and monoclonal antibodies to CD3 (1:100; clone F7.2.38; Dako) and CD19 (1:100; clone LE-CD19; Dako) were used as first-step reagents. Negative controls were done by omitting the primary antibody. As a detection system, we used the EnVision Kit (Dako) according to standard protocols.

Cell preparations. We obtained concentrated leukocyte-depleted erythrocyte and thrombocyte preparations from the German Red Cross Blood Service Baden-Wuerttemberg-Hessen. Cells were washed and lysed in lysis buffer (50 mM Tris HCl pH 8.0, 62.5 mM EDTA pH 7.96, 1% Nonidet P-40, 0.4% Na-deoxycholate) for 30 min at 4 °C. After centrifugation, the supernatant was used for protein blotting. We isolated peripheral blood mononuclear cells with Ficoll-Lymphoprep (Fresenius); we then resuspended the sediment of the Ficoll preparation in PBS and added an equal volume of a 4% Dextrane T-250 solution (Roth). Contaminating erythrocytes were allowed to sediment over a period of 30 min at 21 °C. To increase granulocyte purity, we pelleted the cells of the supernatant and lysed residual erythrocytes by hypotonic shock.

After washing in PBS, 1×10^8 MNCs were incubated for 5 min at room temperature in 2 ml PBS substituted with 30 µl human IgG (16% Beriglobin, see **Supplementary Table 4** online). We added 100 µl of antibodies to CD3, CD14 and CD19 and 60 µl of antibody to CD56 and sorted the MNCs on a FACSAria cell sorting system (Becton Dickinson). At least 2×10^6 cells were collected per fraction. Purity after sorting was as follows: CD3 > 98%, CD14 > 99%, CD19 > 99% and CD56 > 91%. Cells were washed and cells of independent donors were pooled, pelleted and suspended in lysis buffer. Granulocytes were stained independently with 100 µl antibody to CD66b and sorted to a purity of >99%.

Protein blotting. We loaded 10 µg protein per lane on a 15% SDS gel (5 µg for bone marrow MNC preparations). After separation, staining was done with a 2.5% Coomassie solution or the proteins were blotted semi-dry on an Immobilon-P membrane (Millipore). First antibodies (**Supplementary Table 4**) were diluted 1 in 1,000 (anti-HPRT, 1 in 500); secondary antibodies were diluted 1 in 3,000 (dilutions in 10 mM Tris HCl pH 7.5, 150 mM NaCl, 0.05% Tween 20 and 5% milk powder). We developed the blots with Super Script West Pico Chemoluminescent Substrate Kit according to the manufacturer's procedures (ThermoScientific).

Microinjection in zebrafish. The sequence of the morpholino used for *ak2* was 5′-CATCCAGCTACAAATGAGAAACAGC. We injected the morpholinos into the yolk of zebrafish embryos at one- to two-cell stage at a concentration of 0.2 mM.

Whole-mount *in situ* hybridization and RNA probes. We carried out whole-mount *in situ* RNA hybridization of zebrafish targeted with a morpholino to the splice acceptor site of intron 3, mimicking the situation in subject F3P1. *ak2* cDNAs from morphants showed exclusion of exon 4 sequences, resulting in a frameshift mutation (data not shown). Whole-mount *in situ* hybridization was done as described[18]. We synthesized antisense RNA for zebrafish *ak2* from nucleotide 65 to 1128 (NM_212596). All other probes were essentially as previously described[19].

RT-PCR of zebrafish *ak2* RNA. For the amplification of zebrafish *ak2*, we used a forward primer of nucleotides 65 to 85 and a reverse primer of nucleotides 1108 to 1128 (NM_212596).

Apoptosis, mitochondrial transmembrane potential and ROS analyses. Methods for quantitative determination of apoptosis, cytofluorometric analysis of mitochondrial transmembrane potential ($\Delta\psi$) with 3,3′-dihexyloxacarbocyanine iodide ($DiOC_6(3)$) and ROS generation with dihydroethidine (HE) were done as described[20].

Mitochondrial DNA analysis. For mitochondrial PCR analyses and control *AK1* exon 2 amplifications, total genomic DNA was used and amplified with primer pairs specified in **Supplementary Figure 7** and **Supplementary Table 3**.

Accession codes. GenBank RefSeq DNA: *AK2* isoformA, NM_001625.2; *AK2* isoformB, NM_013411.3. RefSeq peptide: AK2 isoformA, NP_001616; AK2 isoformB, NP_037543.

Note: Supplementary information is available on the Nature Genetics website.

ACKNOWLEDGMENTS

We acknowledge the technical assistance of S. Braun, I. Janz, K. Heinrich, T. Kersten and S. Radecke. We are grateful to M. Schorpp for helpful advice. These studies were supported by the German Red Cross Blood Service Baden-Wuerttemberg-Hessen to K.S., the Deutsche Forschungsgemeinschaft (SFB620) and the Max-Planck Society to T.B.

AUTHOR CONTRIBUTIONS

U.P., M.H., T.B. and K.S. designed the study. M.H., A.S. and W.F. cared for the subjects, collected clinical data and performed immunophenotyping. I.H. and T.B. contributed the zebrafish *in situ* hybridizations. K.H. performed and K.H. and K.S. analyzed the chip experiments. U.P., M.H., E.-M.R. and K.S. worked on the RT-PCR screen, the molecular and expression data and on mitochondrial analyses. C.F. performed the apoptosis, mitochondrial membrane potential and ROS assays. T.F.B. collected the immunohistochemistry data. E.-M.R. and M.T.R. did the FACS sorting. U.P., M.H., T.B. and K.S. wrote the paper.

Published online at http://www.nature.com/naturegenetics/
Reprints and permissions information is available online at http://npg.nature.com/reprintsandpermissions/

1. Geha, R.S. *et al.* Primary immunodeficiency diseases: an update from the International Union of Immunological Societies Primary Immunodeficiency Diseases Classification Committee. *J. Allergy Clin. Immunol.* **120**, 776–794 (2007).
2. Alonso, K., Dew, J.M. & Starke, W.R. Thymic alymphoplasia and congenital aleukocytosis (reticular dysgenesia). *Arch. Pathol.* **94**, 179–183 (1972).
3. de Vaal, O. & Seynhaeve, V. Reticular dysgenesia. *Lancet* **2**, 1123–1125 (1959).
4. Emile, J.F., Durandy, A., Le Deist, F., Fischer, A. & Brousse, N. Epidermal Langerhans' cells in children with primary T-cell immune deficiencies. *J. Pathol.* **183**, 70–74 (1997).
5. Espanol, T. *et al.* Reticular dysgenesis: report of two brothers. *Clin. Exp. Immunol.* **38**, 615–620 (1979).
6. Gitlin, D., Vawter, G. & Craig, J.M. Thymic alymphoplasia and congenital aleukocytosis. *Pediatrics* **33**, 184–192 (1964).
7. Haas, R.J. *et al.* Congenital immunodeficiency and agranulocytosis (reticular dysgenesia). *Acta Paediatr. Scand.* **66**, 279–283 (1977).
8. Ownby, D.R., Pizzo, S., Blackmon, L., Gall, S.A. & Buckley, R.H. Severe combined immunodeficiency with leukopenia (reticular dysgenesis) in siblings: immunologic and histopathologic findings. *J. Pediatr.* **89**, 382–387 (1976).
9. DiMauro, S. & Schon, E.A. Mitochondrial respiratory-chain diseases. *N. Engl. J. Med.* **348**, 2656–2668 (2003).
10. Wallace, D.C. Mouse models for mitochondrial disease. *Am. J. Med. Genet.* **106**, 71–93 (2001).
11. Dzeja, P.P. & Terzic, A. Phosphotransfer networks and cellular energetics. *J. Exp. Biol.* **206**, 2039–2047 (2003).
12. Schlauderer, G.J., Proba, K. & Schulz, G.E. Structure of a mutant adenylate kinase ligated with an ATP-analogue showing domain closure over ATP. *J. Mol. Biol.* **256**, 223–227 (1996).
13. Small, T.N. *et al.* Association of reticular dysgenesis (thymic alymphoplasia and congenital aleukocytosis) with bilateral sensorineural deafness. *J. Pediatr.* **135**, 387–389 (1999).
14. Chandra, D. *et al.* Intracellular nucleotides act as critical prosurvival factors by binding to cytochrome C and inhibiting apoptosome. *Cell* **125**, 1333–1346 (2006).
15. Riedl, S.J., Li, W., Chao, Y., Schwarzenbacher, R. & Shi, Y. Structure of the apoptotic protease-activating factor 1 bound to ADP. *Nature* **434**, 926–933 (2005).
16. Krishnan, K.J. *et al.* What causes mitochondrial DNA deletions in human cells? *Nat. Genet.* **40**, 275–279 (2008).
17. Müller, A., Holzmann, K. & Kestler, K. Visualization of genomic aberrations using Affymetrix SNP arrays. *Bioinformatics* **23**, 496–497 (2007).
18. Oxtoby, E. & Jowett, T. Cloning of the zebrafish krox-20 gene (krx-20) and its expression during hindbrain development. *Nucleic Acids Res.* **21**, 1087–1095 (1993).
19. Schorpp, M. *et al.* Conserved functions of Ikaros in vertebrate lymphocyte development: genetic evidence for distinct larval and adult phases of T cell development and two lineages of B cells in zebrafish. *J. Immunol.* **177**, 2463–2476 (2006).
20. Friesen, C., Kiess, Y. & Debatin, K.M. A critical role of glutathione in determining apoptosis sensitivity and resistance in leukemia cells. *Cell Death Differ.* **11**, S73–S85 (2004).